THE FORWARD-FACING FIN – AN UNUSUAL HYDRODYNAMIC DESIGN

M. G. Mungal
Mechanical Engineering Department
Santa Clara University
Santa Clara, CA USA
mgmungal@scu.edu

Tioga Benner
Mechanical Engineering Department
Santa Clara University
Santa Clara, CA USA
tbenner@alumni.scu.edu

ABSTRACT

Motivated by the surprising existence of forward-facing fins in some tropical fish, we investigate their hydrodynamic behaviour at low aspect ratio and moderate Reynolds numbers from low to high angles of attack. Computations using STAR-CCM+ and related wind tunnel experiments reveal a complex flow field with positive and negative shed vortices, and an important trapped stall bubble. The forward-facing fin, either in single or tandem configurations, shows a smooth lift curve vs. angle of attack ("rolling stall"), while the backward-facing fin exhibits sudden lift decrease ("classical stall"), while the straight fin shows a "two-time stall" behaviour previously reported by others. Experimental surface flow visualizations in such highly separated flows are rich in detail and were crucial in the choice of the k-omega turbulence model used in the simulations, while the corresponding surface pressure distribution lacks such detail and is seen to be smooth and relatively benign.

INTRODUCTION AND BACKGROUND

Bioinspired flows have received increasing attention in the last several years (Fish & Launder, 2006), with the Humpback whale flipper showing surface vortices shed from leading edge tubercles which extend the lift and drag performance of the flipper (Fish et al., 2011). The present study is motivated by the surgeonfish family Acanthuridae which have spines, either single or multiple, Fig. 1, that are quite sharp and extend outwards pointing towards the fish's head (Winterbottom, 1971), which are used for aggressive and defensive behaviors (Schober & Ditrich, 1992). Given the unusual forward orientation of the fins, we conjecture that shed vorticity, both positive and negative, from the various fin orientations – i.e. upstream or downstream facing - will lead to differing hydrodynamic behaviors. A straight fin is included in the present study for comparison. While the Reynolds number for the fish are estimated to be relatively low, we investigate the flow behavior at moderate Reynolds numbers that might occur in practical applications (e.g. surfboards).

Figure 1. Picture of Orangespine Unicorn Fish spines with two forward-facing pointed fins. https://www.projectnoah.org/spottings/5391098/fullscreen.

Related past works are those of Van Dam (1987), Van Dam et al. (1991) and Ardonceau (1994) who suggest modest aerodynamic improvements for backward-pointing wings, termed "crescent wings," when compared to unswept elliptical wings. These crescent wings resemble the backward-pointing fin studied here and are more commonly seen on some ("lunate") fish tails. The term crescent wing had been used earlier by Lee (1955) for sweptback wings of a segmented design with differing sweep angles. Forward swept wings were used in the Grumman X-29 aircraft to improve aerobatic performance, but with the drawback of negative aeroelastic stability. In the original crescent wing concept of Lee (1955) and the X-29, both applications use wings of higher aspect ratio, and tend to have straight edges. The present study is oriented more towards low aspect ratios and uses upstream and downstream curved wing edges.

Model fins, Fig. 2, with root cord length of 7 in, a span of 1.3 chords (9.1 in) and a thickness of 1/10 of a chord (.7 in), for an aspect ratio of ~2 were designed in SolidWorks and investigated using the STAR-CCM+ code, with a segmented flow model and k-omega turbulence model at a *Re* of 2 x 10^5 based on root chord for both rounded tips and pointed tips. The fin was set in a large box of size 50 inch width by 50 inch length in the streamwise direction with a height of 25 inch in the fin direction with a uniform water flow inlet of 1 m/s and solid wall boundary conditions. To circumvent a difficulty in SolidWorks the leading edge was an ellipse with a major axis of 5 in and a minor axis of 0.7 in (the thickness of the fin). The trailing edge was a spline curve set to be horizontal when it meets the ellipse. Furthermore, we adopted 0.35 inch radius fillets on the leading edge of both fins resulting in a somewhat more blunt airfoil body, which does impact the findings. We also tested, to a lesser extent, a fin which is more aerodynamic in shape with those results described below and compared to the original fin.

Rigid models of the pointed fin case were 3-D printed using PLA plastic with each fin made of two parts which were epoxied together at roughly the half span location. Experiments were performed in a wind tunnel of 24 in x 24 in x 48 in test section size and maximum speed of 50 m/s with less than 1% free stream velocity variation and turbulence level less than 0.25%. Three nominal speeds of 15.7, 21.0 and 26.2 m/s were used for testing and little Reynolds effect was observed, as would be expected for highly separated flows. Note that in the lift/drag experiments the 9 inch tall fin resides in a portion of the wind tunnel that is 24 in by 12 in inlet size, owing to use of a false wall, so some confinement effects might be felt at the higher angles of attack. In the surface oil flow visualizations the full tunnel size was used, so little confinement effect is expected. The experimental results will be presented after the initial numerical findings are discussed.

RESULTS AND DISCUSSION

Figure 3 for the rounded tip case (left plot) shows typical numerical findings and reveal the three types of behavior seen in this study. The conventional backward-facing fin (blue diamond symbol) shows the sudden stall associated with separation originating off the curved leading edge. The straight fin (green triangle symbol) shows an initial stall, recovery, and then a second stall at much higher angles of attack. This type of behavior has been reported experimentally by Guo et al. (2019) for rigid and flexible finite wings at comparable Reynolds numbers and with similar stall angles for their rigid case. They describe this as a "two-time stall" given the two peaks in the lift coefficient as angle of attack increases. The forward-facing fin (red square symbol), on the other hand, shows a smooth stall behavior (i.e. no sudden drops) over all angles of attack, a behavior we deem "rolling stall," since the lift curve rolls over smoothly from a rising to a falling behavior.

The drag, Fig. 4 (left plot), generally shows two behaviors: a low drag behavior for angles of attack less than 5 degrees, transitioning around 10 degrees, followed by a linearly increasing trend beyond this, most likely associated with the increasing induced drag from the shed vorticity.

Simulation results for the pointed-tip case are also shown in Figs. 3, 4 (right plots). The trends seen for the rounded-tip case are all seen in the pointed-tip case, except at lower levels of lift and drag coefficients. The experimental results will be shown later (Fig. 10) for the pointed-tip case and will be seen to be in reasonably good agreement with the numerical predictions. Hence, the computational results will now be used to infer the flow physics in greater detail. All subsequent discussions will not include the rounded-tip case for brevity, and those results are generally consistent with the pointed-tip case to be shown.

Figures 5, 6 shows computational results for the axial velocity and vorticity for the pointed-fin case at various downstream ("Trefftz") planes (1/10, 1 and 2 chord lengths) normal to the main flow direction. The velocity deficit, positive tip vorticity and negative inboard vorticity are seen with the expected eventual dominance of positive vorticity with downstream distance, as expected for a lifting surface. Results for the rounded-tip are not shown but the trends are similar, with the exception that the tip vortex is stronger from the outset when compared to the pointed-tip case. This is to be expected as the rounded-tip case has more lifting surface area near the tip region.

Perhaps the easiest way to understand the flow field is seen in Figs. 7, 8. These show streaklines released from the pressure and suction surfaces of the model i.e. throughout the boundary layer regions of the fin, which are allowed to propagate into the freestream, thus marking vortical fluid behaviour. The 10-degree angle of attack, Fig. 7, shows essentially attached flow for the backward-facing fin, but the beginnings of an inboard separation bubble for the forward-facing fin (and also implying less lift when compared to the backward-pointing case). This is to be contrasted with the 30-degree angle of attack images, Fig. 8, which show that a full separation bubble has appeared for the backward-facing case while the forward-facing separation bubble has grown, both normal to and spanwise towards the tip. We believe it is the appearance of this nearly 2-D separation bubble for the backward-facing fin which first forms at high angles of attack that leads to the sudden stall behaviour. This is contrasted with the 3-D separation bubble for the forward-facing fin which grows continuously from the root region towards the tip region, with increasing angle of attack. Since the bubble growth increases smoothly with angle, this results in the smooth rolling stall behaviour.

It was noted above that some fish species have double forward-facing fins, while some species have single fins. We investigated this effect by simulating fins at spacings of ¼, ½, 1 and 2 chord lengths to determine the interference effect. Figure 9 shows the lift-drag polars for pairs of fins. For backward-facing fins, the interference effect is seen to be significant, depending upon the spacing of the fins, while for forward-facing fins, the interference effect is negligible with essentially a universal curve for all spacings, and in close agreement with the single-fin case. In this sense the forward-facing fin configuration is robust in behaviour when compared to the backward-facing and straight fin cases.

Experiments were performed for only the pointed fin case. For brevity, images of surface tufts consisting of short threads taped to the fin are not shown. Movies of the tufts reveal the highly recirculating, unsteady flow over various parts of the suction surface at high angles of attack, while the tufts are perfectly still, as expected, on the pressure surface.

Figure 10 shows comparisons of the experimental results at 0, 10, 20 and 30 degrees angle of attack with the previous numerical simulations for the backward-facing and forward-facing pointed fin cases. The blue diamond simulations are to be compared with the green diamond measurements and the red square simulations to the purple square measurements. The lift forces were measured using a strain gauge balance over a range of 0 to 70 microstrain, with typical values of 30 microstrain and uncertainties of +/- ½ microstrain. Results were averaged over several seconds given the overall flow unsteadiness at high angles of attack. The agreement in magnitude and trends appears satisfactory lending credence to the computations.

No pressure measurements were made directly on the models, hence we sought additional measures for comparison with the simulations. To this end, Fig. 11 shows the surface separation lines (Lu, 2010) obtained from use of a mixture of rubbing alcohol and chalk dust to simulate traditional surface oil flow visualization. For safety reasons, we were unable to use kerosine as a carrier fluid, and several commonly available liquids (as found in a typical pharmacy) were tried, and this alcohol/chalk mixture proved best and safest in an open circuit wind tunnel environment. For these visualizations, the same forward-facing fin was mounted horizontally on the centerline of the vertical sidewall of the tunnel, and the entire tunnel cross section area was used, hence the blockage effects are minimal.

As the alcohol evaporates three chalk appearances are revealed: smooth, quick-drying regions (indicative of fast flow), rough slow-drying regions (indicative of slow flow), and lines of accumulation indicative of flow separation. The latter are extracted and compared to surface flow visualization using the four turbulence models available in STAR-CCM+: k-omega, k-epsilon, Reynolds Stress Model, and Spalart-Allmaras. The k-omega model showed very good agreement, Fig. 11, while the other three models showed poor agreement as seen in Fig. 12. These computational images are all obtained by releasing surface streaklines for a short elapsed time and then comparing to the surface chalk images. In this sense, the short streaklines shown here are the beginnings, or footprint, of the long streaklines shown earlier in Fig. 8, the only difference being that in Fig. 8 the

streaklines are allowed to develop for a much longer time, evolving into the main flow, thus marking the downstream vortical fluid. To the extent that the k-omega model captured the surface flow patterns, it was used as the model of choice in all the reported results described above. It is also implicit in our thinking that since the complex flow features close the surface are captured via the k-omega model, then the flow features away from the fin, which are less demanding computationally, are then representative of the time-averaged flow features. Additionally, the surface pressure distributions are also shown in Fig. 13 and, as expected, show none of the details and richness of the suction surface flow behaviour seen in the separation lines of Fig. 11.

Finally, to investigate a more aerodynamic fin, we performed computations for the fin shown (inset) in Fig. 14. Here elliptical surfaces were applied to the leading edge for a fin that more closely represents a practical fin shape. Figure 14 shows results for this more aerodynamic fin when compared to the earlier (less aerodynamic) pointed fin. As can be seen, the more aerodynamic fin shows a more marked catastrophic stall behaviour for the backward-facing fin, as might be expected, while it continues to show the smooth rolling stall behaviour of the forward-facing fin. Interestingly the backward fin case shows a maximum lift coefficient of 0.85, comparable to the maximum value of 0.90 found experimentally by Ardonceau (1994) for a crescent wing aspect ratio of 5, i.e. equivalent to a backward-facing pointed fin of aspect ratio 2.5.

CONCLUSIONS

In this study numerical simulations, supported by wind tunnel experiments show that backward facing fins show a classical stall behaviour that is sudden and occurs at a high angle of attack. This behaviour is consistent with experimental results for earlier crescent shaped wings. Straight fins reveal a two-time stall behaviour previously reported by others. The new forward-facing fins reveal a gentle rolling stall behaviour, to higher angles of attack, with no sudden drops. The numerical simulations suggest that these behaviours are a result of a trapped spanwise stall bubble which forms on the suction side of the fin: suddenly in the backward-facing fin case, but growing slowly outward in the forward-facing fin case. Simulation of a more aerodynamic fin accentuated these differences in behaviour. In addition, simulations of two inline fins of various separations suggest that forward-facing fins are quite insensitive to separation distances and are thus robust in behaviour, suggesting no performance penalty, while backward-facing fins show a strong dependence on separation distance. Finally, experimental surface flow visualization (alcohol/chalk), and not the pressure field, was seen to be instrumental in the choice of the k-omega turbulence model for this flow application, and not the other turbulence models available in the STAR-CCM+ code. Finally, we conjecture that since some birds (e.g. owls) hold their wings in a forward fin configuration at high angles of attack during hunting and landing, they likely benefit from rolling stall i.e. no sudden stall, as seen here. For future work it would be beneficial to perform simulations at higher numerical accuracy given the limitations of the current code.

ACKNOWLEDGEMENTS

This work was supported by a Kuehler grant from Santa Clara University. We thank Jason Chong from the Engineering Computing Center and Anne Mahacek of the Maker Lab for assistance.

REFERENCES

Ardonceau, P. L. “Aerodynamic Properties of Crescent Wing Planforms,” *J. Aircraft*, 31(2), 462-465, 1994.

Fish, F. E., and Lauder, G. V. “Passive and active flow control by swimming fishes and mammals.” *Ann. Rev. Fluid Mech*., 38, 193–224, 2006.

Fish, F. E., Weber, P. W., Murray, M. M., and Howle, L. E. “The Tubercles on Humpback Whales' Flippers: Application of Bio-Inspired Technology,” *Integrative and Comparative Biology*, 51 (1), 203-213, 2011.

Guo, Q., Wang, Z., and Wang, J., “Effects of Flexible Wing on the Aerodynamic Performance of Aircraft”, *13th International Symposium on Particle Image Velocimetry – ISPIV 2019*, Munich, Germany, July 22-24, 2019.

Lee, G. H., “The Aerodynamic and Aeroelastic Characteristics of the Crescent Wing,” *The Aeronautical Journal* , Volume 59 , Issue 529 , pp. 37 – 44, January 1955.

Lu, F. K., “Surface Oil Flow Visualization – Still Useful After All These Years,” *Eur. Phys. J. Special Topics 182*, 51–63, 2010.

NASA Armstrong Fact Sheet: X-29 Advanced Technology Demonstrator Aircraft https://www.nasa.gov/ centers/armstrong/news/FactSheets/FS-008-DFRC.html

Schober, U.M., and Ditrich, H., “Anatomy and Use of the Caudal Spine in the Aggressive Behavior of a Surgeonfish (Osteichthyes: Acanthuridae),” *Marine and Freshwater Behavior and Psychology*, 21 (4), 277-284, 1992.

Van Dam, C. P. “Induced-Drag Characteristics of Crescent-Moon-Shaped Wings,” *J. Aircraft*, 24 (2), 115-119, 1987.

Van Dam, C. P,, Vijgen, P. M. H. W., and Holmes, B. J. “Experimental Investigation on the Effect of Crescent Planform on Lift and Drag,” *J. Aircraft*, 28 (11), 713-720, 1991.

Winterbottom, R., “Movement of the Caudal Spine of Some Surgeonfishes (Acanthuridae, Perciformes).” *Copeia*, Vol. 1971, No. 3, pp. 562-566, 1971.

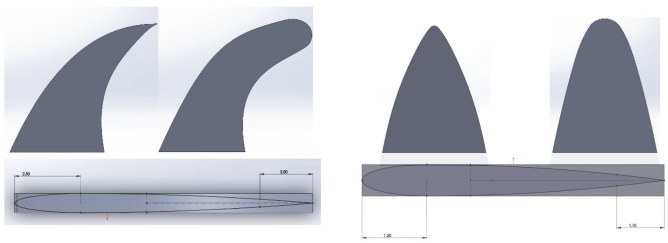

Figure 2. Left: Planform sections of pointed and rounded fins and sketch of the airfoil shape from the side for forward and backward swept fins. Right: Pointed and rounded straight fin showing planform and side airfoil shape

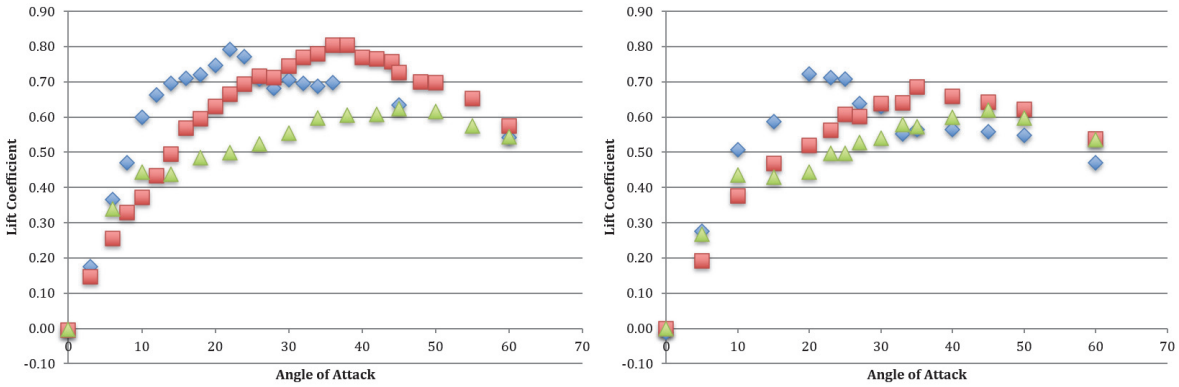

Figure 3. Lift coefficients of fins at different angles of attack. Left – rounded fins, Right - pointed fins. Symbols: blue diamond – backward fin, red square – forward fin, green triangle – straight fin.

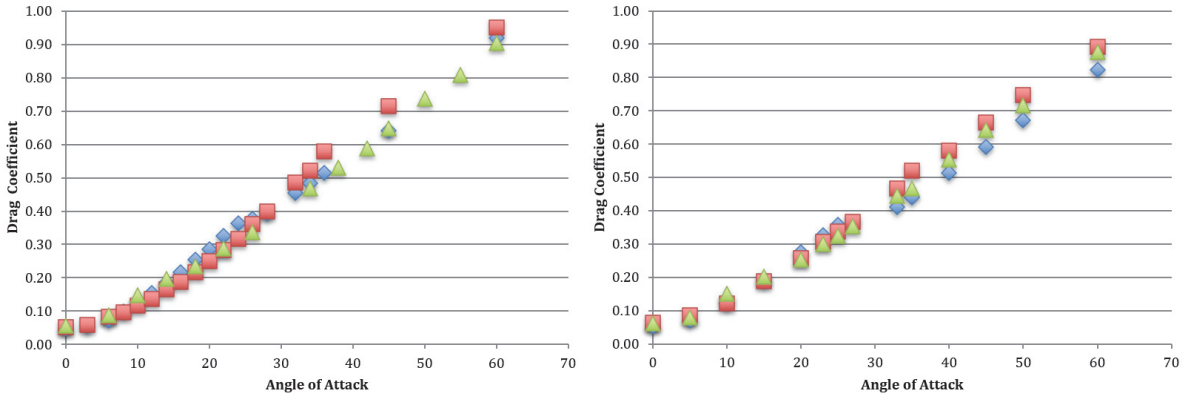

Figure 4. Drag coefficients of fins at different angles of attack. Left – rounded fins, Right - pointed fins. Symbols: blue diamond – backward fin, red square – forward fin, green triangle – straight fin.

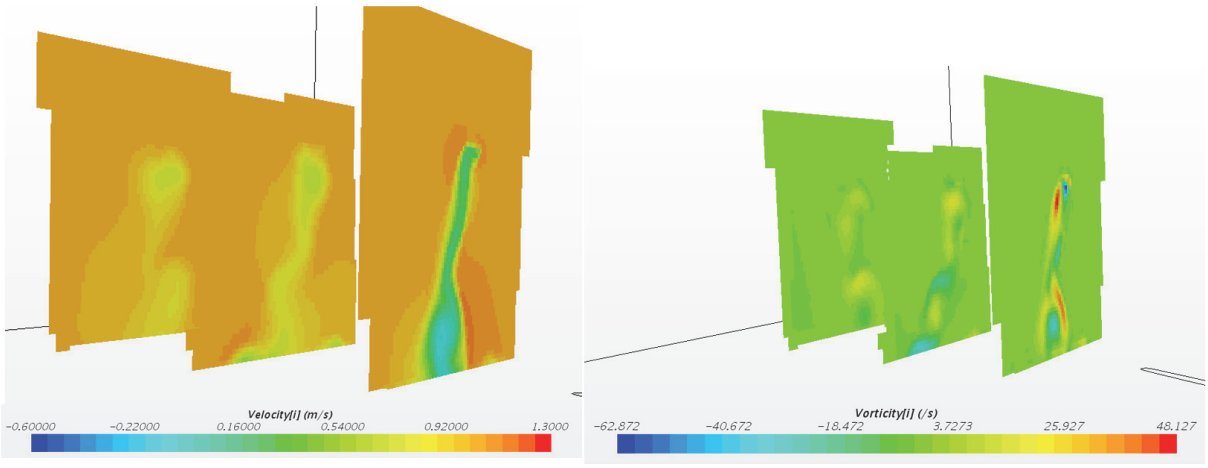

Figure 5. Axial velocity (left) and streamwise vorticity (right) of backward-facing pointed fin at 30 degrees angle of attack.

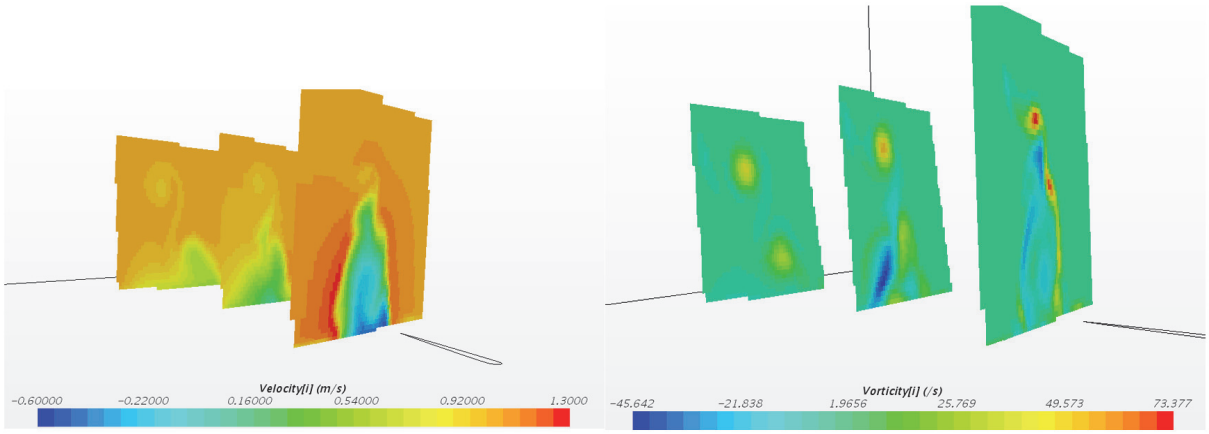

Figure 6. Axial velocity (left) and streamwise vorticity (right) of forward-facing pointed fin at 30 degrees angle of attack.

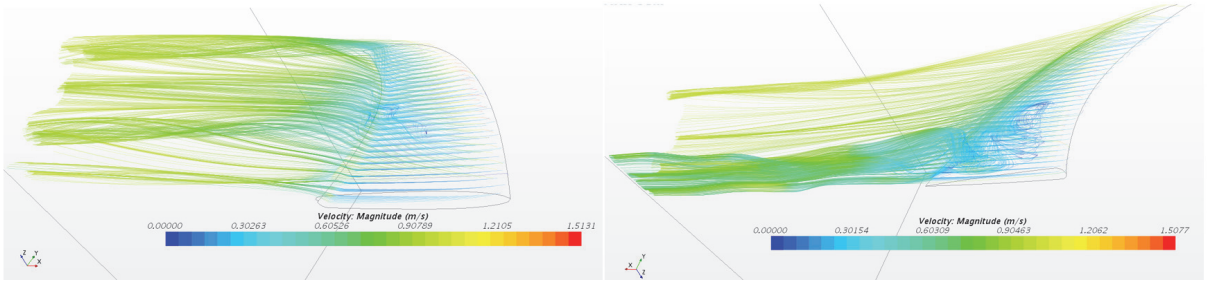

Figure 7. Long streaklines from surfaces of backward-facing pointed fin (left) and forward-facing pointed fin (right) at 10 degrees angle of attack. Flow is right to left.

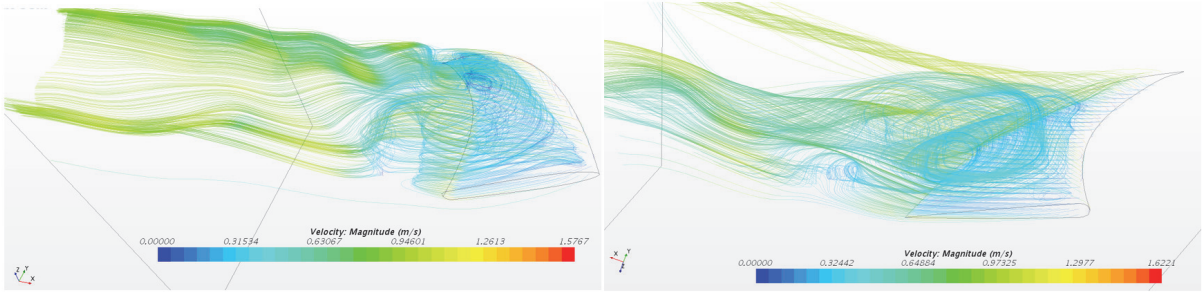

Figure 8. Long streaklines from surfaces of backward-facing pointed fin (left) and forward-facing pointed fin (right) at 30 degrees angle of attack. Flow is right to left.

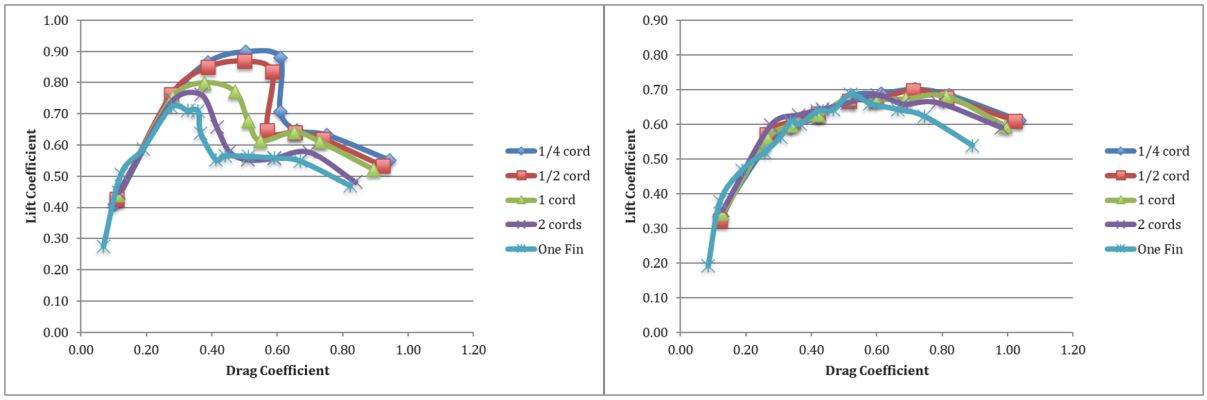

Figure 9. Lift-drag polars for inline pointed fins at various separations. Left: backward-facing. Right: forward-facing.

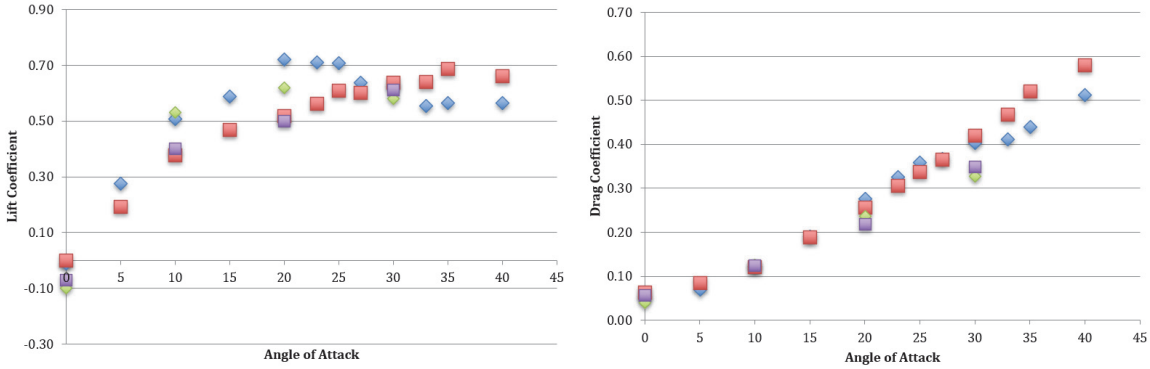

Figure 10. Lift and Drag Coefficients of forward-facing pointed fin with experimental measurements (green, purple points).

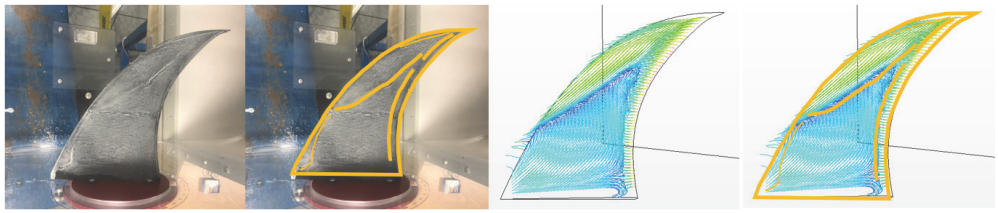

Figure 11. Comparison of suction surface flow patterns, forward-facing pointed fin at 30 degree angle of attack. Flow is right to left. Left pair: Experimental surface flow measurements. Right pair: k-omega surface flow predictions. Orange separation lines are transferred from experiments to flow predictions.

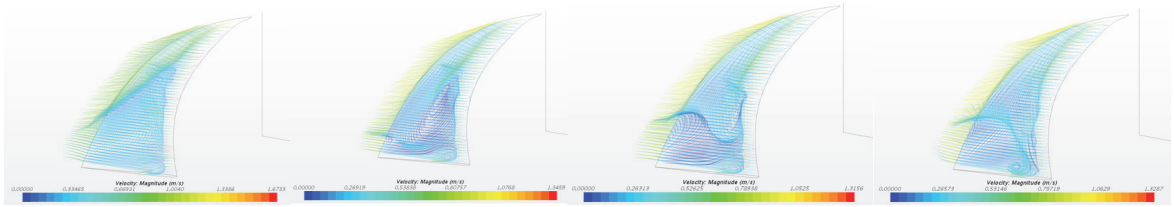

Figure 12. Comparison of short surface streaklines for four turbulence models at 30 degree angle of attack. Left to right: k-omega, k-epsilon, Reynolds Stress Model, Spalart-Allmaras.

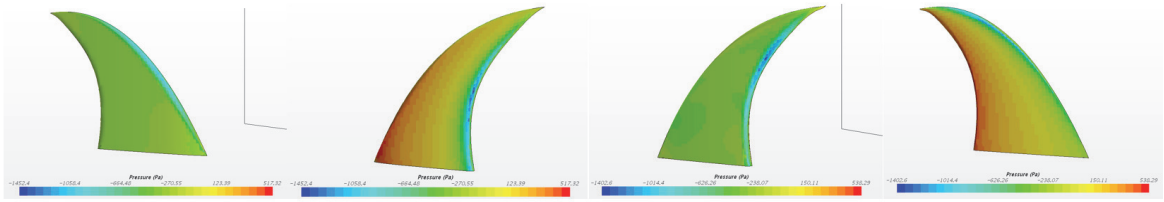

Figure 13. Surface pressure for pointed fins at 30 degree angle of attack. Left pair: backward-facing fin, suction (left) and pressure (right) surfaces shown. Right pair: forward facing fin, suction (left) and pressure (right) surfaces shown.

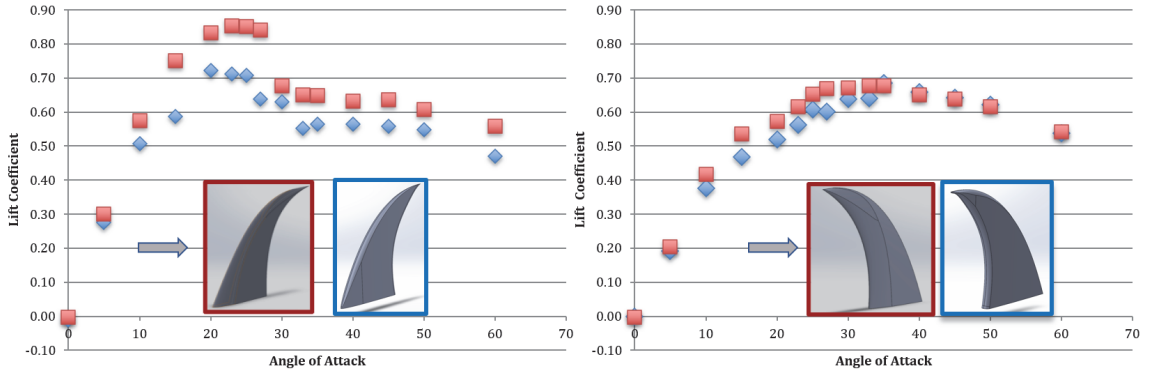

Figure 14. Comparison of more aerodynamic fin (red squares, red inset image) with previous less aerodynamic fin (blue diamonds, blue inset image). Left: Backward-facing pointed fin. Right: Forward-facing pointed fin